Total flavones from *Sceptridium ternatum* alleviate pulmonary hypertension through inhibiting the proliferation of vascular endothelial cells

Qinglin Li[1], Wenxiu Xin[1], Haiyin Ding[1], Yiwen Zhang[2,3], Xiaowei Zheng[2,3], Yujia Liu[2], Ping Huang[2,3]

[1]Cancer Hospital of the University of Chinese Academy of Sciences (Zhejiang Cancer Hospital), Hangzhou, China; [2]Clinical Pharmacy Center, Department of Pharmacy, Zhejiang Provincial People's Hospital (People's Hospital of Hangzhou Medical College), Hangzhou, China; [3]Key Laboratory of Endocrine Gland Diseases of Zhejiang Province, Hangzhou, China

Contributions: (I) Conception and design: Q Li, W Xin, Y Liu; (II) Administrative support: P Huang; (III) Provision of study materials or patients: X Zheng; (IV) Collection and assembly of data: H Ding; (V) Data analysis and interpretation: P Huang; (VI) Manuscript writing: All authors; (VII) Final approval of manuscript: All authors.

Correspondence to: Ping Huang. Clinical Pharmacy Center, Department of Pharmacy, Zhejiang Provincial People's Hospital (People's Hospital of Hangzhou Medical College), 1 Banshan Road, Hangzhou 310022, China. Email: huangping1841@zjcc.org.cn.

Background: *Sceptridium ternatum* is a traditional Chinese medicine that is prescribed to treat respiratory diseases in China. Our previous study confirmed that total flavones from *Sceptridium ternatum* (FST) have preventive and therapeutic effects on pulmonary hypertension (PH). The present study sought to investigate the mechanism underpinning the therapeutic efficacy of FST in PH.

Methods: Cell Counting Kit-8 (CCK-8) and 5-ethynyl-2'-deoxyuridine (EdU) assays, real-time quantitative PCR (RT-qPCR), western blot, flow cytometry, high-throughput sequencing, and bioinformatics analysis were performed to study the therapeutic mechanism of FST in PH at the gene, cell, and animal levels.

Results: The results showed that FST could inhibit the proliferation of both human pulmonary artery smooth muscle cells (HPASMCs) and human pulmonary microvascular endothelial cells (HPMECs), and downregulate the expression of HIF1α and HIF2α, which are the key factors in the pathogenesis and occurrence of PH. FST could also inhibit the activation of the downstream JAK2-STAT3 signaling pathway and upregulate the expression of the negative regulator SOCS1. Vascular endothelial cell and smooth muscle cell proliferation was inhibited and the symptoms of PH were relieved by FST.

Conclusions: The findings of this study offer important clues for the identification of new molecular targets in FST treatment and the development of treatment strategies for PH.

Keywords: Total flavones; pulmonary hypertension (PH); HIF-α; JAK2-STAT3; *Sceptridium ternatum*

Introduction

Pulmonary hypertension (PH) is a devastating disease and an important step in the pathogeneses of chronic mountain sickness and chronic pulmonary heart disease. PH features a continuous increase in pulmonary artery pressure, which can lead to right-sided heart failure and death (1). The pathogenesis of PH is complex, and the occurrence of PH is associated with BMPR2 mutation, impaired BMPR-II signaling, single-nucleotide polymorphisms (SNPs) of SERT and TRPC6, epigenetic sex hormone imbalance, Mitochondrial metabolic dysfunction and so on (2). The pathophysiological basis for the progressive development of pulmonary vascular lesions is pulmonary vascular remodeling, which is correlated with the proliferation/apoptosis imbalance of pulmonary artery smooth muscle cells (PASMCs) (3). Inhibiting the proliferation and

inducing the apoptosis of PASMCs can improve pulmonary vascular remodeling and reduce pulmonary artery pressure.

The main clinical treatments for PH include supportive treatment, targeted drug therapy, interventional therapy, and surgical treatment. Interventional therapy is used to treat PH caused by congenital heart disease, while surgery is the preferred treatment for chronic thromboembolic PH. For patients with PH for whom medication is ineffective, lung transplantation is always recommended (4). Medications which dilate pulmonary arteries and improve pulmonary vascular resistance and pulmonary function, such as prostaglandin E, sildenafil, bosentan, and nitric oxide, can effectively relieve the symptoms of PH. Sildenafil has the effect of expanding the pulmonary arteries and improving both the pulmonary vascular resistance and pulmonary function of the patient; thus, it can effectively relieve the symptoms of PH. However, the above-mentioned medications are only symptomatic treatments, and they cannot reverse pulmonary vascular remodeling or improve the prognosis (5,6). Therefore, developing new drugs that are safe and effective and understanding their explicit mechanisms is important for the treatment of PH.

Sceptridium ternatum is a traditional Chinese medicine that has been found to have an antitoxic effect in the body. It is prescribed in the treatment of respiratory diseases. In the preliminary study by our research team, a rat model of monocrotaline (MCT)-induced PH was built, and total flavones from *Sceptridium ternatum* (FST) were given to the model rats. Results showed that FST reduced the right ventricular pressure (RVP) and mean arterial pressure of the rat model as well as the pulmonary and right ventricular hypertrophy (RVH) indexes. In addition, FST has also been reported to displayed certain preventive and treatment effects against PH and heart disease (7). Further study indicated that FST inhibited the proliferation of PASMCs and the NF-κB signaling pathway, which influenced the transcription of inflammatory cells and prevented vascular inflammation.

In our previous study, we adopted an MCT rat model to support the claim that FST treatment could alleviate PH, but the working mechanism remained unclear. Therefore, the present study sought to investigate the mechanism of the therapeutic efficacy of FST in PH. We present the following article in accordance with the ARRIVE reporting checklist (available at https://atm.amegroups.com/article/view/10.21037/atm-21-5889/rc).

Methods

Cells and animals

Human PASMCs (HPASMCs) and human pulmonary microvascular endothelial cells (HPMECs) were purchased from Biological Science and Technology Co., Ltd. (Guangzhou, China). To maintain biological stability, the cell conduction algebra was maintained within 15 generations. Forty-eight specific-pathogen-free (SPF) male Sprague-Dawley (SD) rats were purchased from SIPPR/BK Experimental Animal Co., Ltd. Experiments involving animals were performed under a project license (No. 0273015) granted by the ethics institutional review board of Zhejiang Cancer Hospital, in compliance with Regulations for the Administration of Affairs Concerning Experimental Animals (modified in 2017) for the care and use of animals. The rats were maintained under SPF conditions. All assessments were evaluated by the investigator who was blind to the treatment groups.

Medicines and reagents

Sceptridium ternatum Herba was collected from Lishui, Zhejiang, China. Voucher specimens were identified by Prof. Xilin Chen of Zhejiang Chinese Medicine University. A voucher specimen of *Sceptridium ternatum* was deposited in the herbarium of the College of Pharmacy, Zhejiang Chinese Medical University (Hangzhou, China; 310053).

β-actin was purchased from Sigma Co., Ltd. (St. Louis, MO, USA). HIF1α, STAT3, p-STAT3, JAK2, p-JAK2, and SOCS1 were obtained from Abcam Co., Ltd. (Cambridge, MA, USA). Horseradish peroxidase-labeled Goat anti-Rabbit IgG and Goat anti-Mouse IgG were purchased from Beijing Zhongshan Jinqiao Co., Ltd. (Beijing, China). For western blot, 30% acrylamide/Bis (29:1), ammonium sulfate, twelve sodium dodecyl sulfate, N,N,N',N'-tetramethylethyle nediamine (TEMED), and western blot membrane washing solution were purchased from Shanghai Beyotime Biotechnology Co., Ltd. (Shanghai, China). For real-time quantitative PCR (RT-qPCR), primers were obtained from Shanghai Sangon Biological Technology Service Co., Ltd. (Shanghai, China). The RNA extraction reagent TriZol was purchased from Bio RT Reagent Kit Co., Ltd. (Vancouver, Canada). PrimeScript™ (Perfect Real Time) was supplied by Bao Biotechnology Co., Ltd. (Dalian, China).

Table 1 High-resolution mass spectrometry data and elemental composition of 19 flavonoids from FST

Retention time (min)	Molecular formula	[M-H]⁻	ppm	Chemical compound
18.6	$C_{27}H_{30}O_{16}$	609.1461	0	Quercetin-3-O-rhamnose-7-O-glucoside
21.4	$C_{39}H_{50}O_{25}$	917.2568	1.6	Kaempferol-3-O-two-7-O-glucose glucose rhamnoside
24.1	$C_{33}H_{40}O_{20}$	755.205	1.3	Kaempferol-3-O-7-O-glucose rhamnoside
24.6	$C_{27}H_{30}O_{15}$	593.1512	0	Kaempferol-3-O-rhamnose-7-O-glucoside
29.1	$C_{26}H_{28}O_{14}$	609.1457	0.7	Kaempferol-3-O-glucose-7-O-glucoside
32.1	$C_{21}H_{20}O_{12}$	463.0877	1.1	Quercetin 3-O-glucoside
35.1	$C_{48}H_{54}O_{27}$	1,063.293	0.5	Quercetin-3-O-(2, 3-two-O-4-glucose) -rhamnolipid
36.6	$C_{33}H_{40}O_{20}$	755.2049	1.2	Quercetin-3-O-(–)-glycosyl glucoside
39.0	$C_{42}H_{46}O_{22}$	901.2402	–0.6	Ternatumoside XIII
39.5	$C_{29}H_{32}O_{17}$	651.1557	1.5	Quercetin-3-O-rhamnose-7-O-acetyl glucoside
40.2	$C_{39}H_{50}O_{24}$	901.2602	1.9	Ternatumoside III
42.6	$C_{36}H_{36}O_{17}$	739.2069	–3.1	Kaempferol-3-O-glucose l-rhamnosyl-7-O-rhamnoside
44.1	$C_{34}H_{40}O_{19}$	797.2132	1.7	Kaempferol-3-O-glucose rhamnose-7-O-acetyl glucoside
45.1	$C_{27}H_{30}O_{14}$	577.1539	4.1	Kaempferol-3-O-rhamnose-7-O-rhamnoside
46.3	$C_{57}H_{62}O_{29}$	1,209.3209	2.1	Ternatumoside VI
46.4	$C_{21}H_{20}O_{11}$	447.0929	0.9	Quercetin-3-O-rhamnolipid
46.5	$C_{51}H_{52}O_{24}$	1,047.2749	0.6	Ternatumoside IV
49.4	$C_{33}H_{40}O_{18}$	723.2128	1.9	Kaempferol-3-O-p-coumaricacid udp-l-rhamnose-7-O-rhamnoside
61.7	$C_{15}H_{10}O_6$	285.0408	1.2	Luteolin
66.0	$C_{21}H_{20}H_{10}$	431.0978	1.3	Kaempferol-3-O-rhamnoside

FST, total flavones from *Sceptridium ternatum*.

Preparation and identification of FST

The FST extraction process was as follows: The *Sceptridium ternatum* were extracted 3 times with 70% ethanol which amount to 6 times the weight of herbs for 2 hours each time. The average FST content was 4.14 mg/g, and the transfer rate was over 90%. FST were purified on polyamide resin through column elution at a flow rate of 2 mL/min with 4 bed volumes (BV) of 70% ethanol. The obtained FST content met the requirements for formulation preparation. The obtained total flavonoid content was 57.12% and the yield exceeded 76%.

Fragmented ions such as [M-Glc-H]⁻, [M-Rha-H]⁻, and [M-Rha-Glc-H]⁻ were detected by negative ion mode mass spectrometry. Accurate element composition was obtained from fragmentation information through multistage mass spectrometry combined with high-resolution mass

spectrometry. The mass spectrometry data and relevant literature show that *Sceptridium ternatum* contains 19 types of flavonoid structure (*Table 1*).

Cell culture

HPASMCs and HPMECs were placed into smooth muscle cell medium containing 10% fetal bovine serum and 100 U/mL penicillin and streptomycin. All cells were inoculated into the culture flask at a dose of 10^5 cells/ml and cultured at 37 ℃ in a 5% CO_2 incubator.

Effects of FST on the expression of HIF1α and HIF2α

To determine whether FST exerts its anti-PH effect via HIF, HPASMCs were treated with FST at different concentrations (2.5 or 5 μg/mL) for 36 hours. RT-

qPCR and western blot were conducted to determine the expression levels of HIF1α mRNA and protein. Additionally, HPMECs were treated with FST (5 μg/mL) for 48 hours, and the protein expression of HIF2α was detected by western blot. Immunohistochemistry was used to examine the effect of FST on HIF1α and HIF2α expression in the lung tissues of rats with PH.

Effects of FST on the proliferation of HPMECs and HPASMCs

Firstly, the effect of FST on the proliferation of HPMECs was detected by 5-ethynyl-2'-deoxyuridine (EdU) assay and then observed by immunofluorescence microscopy. The time curve of FST was used to evidence its anti-PH effect. Finally, HPMECs and HPASMCs were seeded onto 96-well plates at a density of 4,000 cells/well. Cells were left to adhere for 12 hours, after which 5 μg/mL FST was added to incubate for 40 minutes and then 25 μM $CoCl_2$ was added. Cell viability was measured by Cell Counting Kit-8 (CCK-8) assay after 48 hours.

Detection of genes and proteins

Proteins were detected by western blot in this study. RT-qPCR was performed using SYBR1 GreenER qPCR SuperMix (Sigma), and samples were run on the StepPlusOne Real-Time qPCR System (Applied Biosystems). Similar to that in a previously described method (8), the RT-qPCR reaction system consisted of 5 μL complementary DNA, 4.75 μL diethylpyrocarbonate (DEPC) water, 0.25 μL primer, and 10 μL SYBR. The dissolution curve was plotted automatically using the software. The primer sequences used were as follows: β-actin: forward/reverse (5'-3'): CCTCTATCAGTGC/CCTGCTTGCTGATCCACATC; JAK2: forward/reverse (5'-3'): AGTGCTGGAACAACAATG/TTGGTCTCTGAGTGAAGG; STAT3: forward/reverse (5'-3'): GTTGGAGGTGTGAGGTAG/AAGGTCAAGTGGGAAAGG; SOCS1: forward/reverse (5'-3'): AGACCTTCGACTGCCTCTTC/GGAGTACCGGGTTAAGAGGG; SOCS5: forward/reverse (5'-3'): AGCCGAAGTGAGAATGTGGA/GCACAGTTTTGGTTCCGTCT.

In vivo study of FST in rats with MCT-induced PH

The SD rats were randomly divided into the following six groups (n=8 in each group): negative control group, model group (MCT, 60 mg/kg), positive control group (sildenafil, 17 mg/kg), high-dose FST group (500 mg/kg), medium-dose FST group (100 mg/kg), and low-dose FST group (20 mg/kg). The treatments were administered continuously for 21 days. The pulmonary artery systolic pressure (PASP), pulmonary artery diastolic pressure (PADP), mean pulmonary arterial pressure (mPAP), right ventricular systolic pressure (RVSP), mean RVP (mRVP), rat lung weight (LUNG), lung wet weight index (LI), right ventricle (RV), right ventricular mass index (RVMI), and RVH index of rats in each group were observed, as were other physiological indexes. Subsequently, hematoxylin and eosin (HE) staining was used to observe the pulmonary vessel wall thickness and lung morphological structure in the rats.

Gene expression profiling using microarray

Sample preparation

Log-phase PASMCs were inoculated into a 6-well plate and harvested for transfection after reaching 60–80% confluence. The transfected cells were observed under a fluorescence microscope, and the results were verified by western blot. Cells transfected with HIF1α DNA plasmids and empty vectors were treated with FST. Different cell groups were established as follows: transfection with control vectors, transfection with vectors + 2.5 μg/mL FST, transfection with HIF1α DNA plasmids, and transfection with HIF1α DNA plasmids + 2.5 μg/mL FST. Three replicates were set up for each group.

Collection of samples for microarray analysis

Cells transfected with HIF1α DNA plasmids and empty vectors were treated with FST. Different treatment groups were established: control vector group, vector + FST group, HIF1α overexpression group, and HIF1α overexpression + FST group Triplicates were set up for each group. After treatment for 24 hours, TRIzol was added, and microarray analysis was performed as follows. Briefly, the cells were harvested and the supernatant was discarded. Then, the cells were washed with phosphate-buffered saline (PBS), digested in trypsin, centrifuged, and washed with PBS again, before 1 mL TRIzol was added. The cells were gently blown until the liquid became transparent and then preserved at –80 ℃ until use.

Total RNA was extracted from treated cells. The cells were washed twice with PBS and digested in trypsin for 5 minutes. The digested solution was then collected and

centrifuged at 3,000 rpm for 5 minutes, after which the supernatant was discarded, and the cell precipitate was lysed in TRIzol. The cells were washed with chloroform to remove the impurities and dissolved in isopropyl alcohol. Excess solvent was removed by washing with 75% ethanol and left to evaporate. Finally, the RNA precipitate was dissolved in sterilized RNase-free distilled water.

RNA purification and reverse transcription

The extracted RNA was dissolved in 100 µL of sterilized RNase-free distilled water, and buffer RLT (350 µL) and anhydrous ethanol (250 µL) were added. After mixing, the cells were passed through a RNeasy mini-column and centrifuged at 8,000 g for 15–30 seconds. Then, the filtrate was discarded, and 350 µL buffer RW1 was added to the centrifuge column. After centrifugation at 8,000 g for 15 seconds, the filtrate was discarded, and premixed DNase I (10 µL DNase I + 70 µL Buffer RDD) was added to the centrifuge column, which was then left to stand at room temperature for 15 minutes. Subsequently, 350 µL Buffer RW1 was added and centrifuged at 8,000 g for 15 seconds. After the filtrate had been discarded, 500 µL Buffer PRE was added and centrifuged at 8,000 g for 15 seconds. Again, the filtrate was discarded, and 500 µL Buffer PRE was added and centrifuged at 8,000 g for 2 minutes. Finally, the filtrate and casing were discarded, and the RNeasy mini-column was transferred to a clean Eppendorf tube (1.5 mL) for centrifugation, which was conducted at 8,000 g for 1 minute using 40 µL of sterilized RNase-free distilled water. The experiment was repeated twice, and the optical density (OD) value was measured. The purity of the extracted RNA was determined by the OD method, and the purified RNA was reverse-transcribed using the PrimeScript RT Reagent Kit with gDNA Eraser.

Synthesis of labeled complementary RNA by in vitro transcription (IVT)

IVT mixture (30 µL) was added to a tube containing double-stranded complementary DNA and mixed well. The reaction liquid was centrifuged at a low speed and collected in a tube. After incubation in the RT-qPCR system at 40 ℃ for 4–16 hours, the product was purified and preserved at –20 ℃.

Purification of amplified RNA (aRNA)

RNA-conjugated magnetic beads (10 µL) were added into 50 µL of aRNA binding buffer concentrate. Into the sample, aRNA binding buffer (60 µL) and ethanol solution (120 µL) were successively added and gently oscillated for 2 minutes. After proper mixing, the sample was transferred to a U-shaped plate and left to stand on a magnetic rack for 5 minutes. The magnetic beads were collected, 100 µL of aRNA binding buffer was added, and the beads were oscillated for 1 minute. Then, the tube was transferred to the U-shaped plate and left to stand on the magnetic rack for 5 minutes. The supernatant was discarded, and the cells were washed once. Into the tube, 50 µL of aRNA eluent which had been preheated at 50–60 ℃ was added. The U-shaped plate was violently oscillated for 3 minutes until the magnetic beads were completely mixed. Then, the aRNA-conjugated magnetic beads were eluted, and the U-shaped plate was transferred to the magnetic rack and left to stand for about 5 minutes. Finally, the supernatant was transferred to a new tube.

Microarray hybridization, washing, staining, and scanning

The aRNA fragmentation mixture was prepared using a kit and reacted at 94 ℃ for 35 minutes. Then, the cells were immediately placed into an ice bath. The size of the fragmentation products was detected by electrophoresis (approximately 35–200 nt). Hybridization solution was prepared according to the type of microarray used. Pre-hybridization solution was added to the microarray balanced at 25 ℃. The solution was heated at 99 ℃ for 5 minutes, placed at 45 ℃ for 5 minutes, and then added to the microarray. Hybridization was performed at 45 ℃ and 60 rpm for 16 hours. The products were divided into stain1 (600 µL), stain2 (600 µL), and Array Holding Buffer (800 µL), and placed on the workstation. Finally, the stained microarrays were washed and then scanned.

Microarray scan and analysis

Microarrays were scanned with the GeneChip® Scanner 3000 (Cat#00-00212, Affymetrix, Santa Clara, CA, USA).

The raw data were read using Command Console Software 3.1 (Affymetrix). Quality control was performed, and the data were normalized using the MAS5.0 algorithm with Gene Spring Software 11.0 (Agilent Technologies, Santa Clara, CA, USA).

Differentially expressed genes and pathway analysis

Microarray data were assessed using microarray scan images, box plots, and scatter plots. Genes with weak probe signals were excluded. At least one sample with strong probe signals that indicated differentially expressed genes compared with the background was retained out of two samples. The significance threshold was set at ≥3-fold change. The effect of FST on genes related to PASMC proliferation was assessed based on the expression of HIF1α.

Construction of the PH model

Based on body weight (BW), 48 SD rats were divided randomly into six groups (n=8 in each group): negative control group, model group, positive control group (sildenafil citrate, 17 mg/kg), high-dose FST group (500 mg/kg), moderate-dose FST group (100 mg/kg), and low-dose FST group (20 mg/kg). Except for those in the negative control group, the rats were given a single dose of MCT (30 mg/mL) via subcutaneous injection (MCT dissolved in ethanol: normal saline =2:8; dose 60 mg/kg; total volume 2 mL/kg). The negative control group was injected with an equal amount of ethanol-normal saline mixture (2:8) subcutaneously.

Dosing regimens

Three FST dosage groups were established based on the previous study: 20, 100, and 500 mg/kg. The day after the establishment of the PH model, FST administration by gavage commenced at the dosage of 20, 100, or 500 mg/kg. To the positive control group, sildenafil citrate was given at a dose of 17 mg/kg; to the model group and negative control group, an equal amount of normal saline was given. Treatment was administered once daily and continuously for 21 days.

Collection of lung tissue

Lungs were harvested from the rats, and normal saline was injected to the pulmonary artery. The pulmonary hila were removed, and the surface was dried using filter paper. Lung weight was measured using an electronic balance. One-half of the left lung and one half of the right lungs was fixed in 10% paraformaldehyde, and the remaining tissue was preserved at −80 °C. The LI was calculated. LI = LUNG/ BW × 100%.

Immunohistochemical staining of lung tissues

The lung tissue sections were immersed in 500 mL of antigen retrieval buffer and then heated in a microwave at 80 °C for 5 minutes. After that, the sections were cooled to room temperature in a 4 °C fridge. This process was repeated three times. The sections were transferred to a dark box, covered with 3% H_2O_2 for 10 minutes, and then washed three times with PBS, for 3 minutes each time. The sections were incubated with primary antibody at 4 °C overnight and then washed three times with PBS, for 5 minutes each time. The sections were incubated a second time, with secondary antibody at room temperature for 30 minutes, and then washed three times with PBS, for 5 minutes each time. 3,3'-diaminobenzidine (DAB) substrate was added for color development, and the reaction was terminated by washing the sections under running water. Then, the sections were counterstained with hematoxylin for 2 minutes and washed under running water. After dissociation in hydrochloric alcohol solution, the sections were again washed under running water, before being dehydrated using gradient alcohol (80%, 95%, 95%, and 100%). After dehydration in xylene for 10 minutes, the sections were sealed. Finally, the sections were observed under a microscope, and photos were taken.

Statistical analysis

Data were reported as the mean ± standard deviation and were statistically analyzed using SPSS 19.0 software (IBM, New York, NY, USA). Intergroup comparisons were conducted by one-way analysis of variance, and P<0.05 was considered statistically significant.

Results

Effects of FST on RVSP and mRVP in rats with PH

The RVSP and mRVP of the MCT model rats were significantly higher than those in the negative control group (P<0.001). Compared with those in the model

group, the mRVP and RVSP in each FST dose group were significantly decreased, which indicated that FST intervention could reduce the RVSP and mRVP in rats with PH. The antihypertensive effect of FST in the low-dose (20 mg/kg) group was the greatest (P<0.05), and was equal to that of the positive control (sildenafil 17 mg/kg) (*Figure 1A*).

Effects of FST on PASP, PADP, and mPAP in rats with PH

The PASP, PADP, and mPAP of the rats of the MCT model were significantly higher than those in the negative control group (P<0.001), which showed that the PH model had been established successfully. FST (20, 100, and 500 mg/kg) reduced the PASP, PADP, and mPAP in the model rats. The antihypertensive effects of FST were greatest in the low-dose (20 mg/kg) group (P<0.05), and were similar to the effects of the positive control, including the decrease in mPAP (26.88±6.31 *vs.* 28.13±6.01). However, compared with the control group, the value of mPAP in the low-dose (20 mg/kg) group was still slightly higher.

Effects of FST on the pathological structure of lung tissue in rats with PH

To examine the morphological and structural changes to rat lung tissue under FST treatment, HE staining of lung tissue from the rats was performed, and the stained tissues were observed and photographed under an optical microscope. HE staining revealed that the pulmonary arterial wall was thinner in the negative control group than in the other groups. In the model group, the smooth muscle cells of the membrane and pulmonary artery in the small pulmonary artery wall were obviously proliferated, and there was obvious thickening of the small artery wall. Compared to the model group, the FST low-dose (20 mg/kg) and medium-dose (100 mg/kg) groups exhibited decreased small blood vessel wall thickness, but there was no significant change in the FST high-dose group (500 mg/kg). The results showed that the small vessel wall thickness of rats with PH was significantly reduced by FST in the low- and medium-dose groups (*Figure 1B*).

Effects of FST on the expression of HIF1α and HIF2α

As shown in *Figure 2A,2B*, FST effectively inhibited the expression of HIF1α and HIF2α induced by hypoxia (P<0.05). Immunohistochemistry was used to examine the expression of HIF1α and HIF2α in the lung tissues of FST-treated PH rats. As shown in *Figure 2C,2D*, the protein expression of both HIF1α and HIF2α in the lung tissues of PH rats was significantly decreased after treatment with FST 20 mg/kg. The above results indicate that FST alleviated PH via downregulating HIF expression.

Effect of FST on the proliferation of vascular endothelial cells

As shown in *Figure 3*, EdU assay results showed that FST (5 μg/mL) could significantly inhibit the proliferation of HPMECs. Also, in the CCK-8 experiment, FST had an obvious inhibitory effect on HPMEC proliferation, which was significant between 48 and 72 hours. Additionally, $CoCl_2$ was used to establish a hypoxic cell model and interleukin (IL)-6 was used for the promotion of HPASMC proliferation and reverse validation. Once again, FST had a clear and significant inhibitory effect on cell proliferation, and the results are shown in Appendix 1.

Analysis of genes related to HIF1α

After the transfection of PAMSCs with HIF1α plasmids, the expression levels of 1,594 genes, including 988 upregulated genes and 606 downregulated genes, changed significantly (≥3-fold change). Among the significantly downregulated genes, *LEPROT*, *CAST*, and *MFSD6* exhibited the greatest expression changes, with >50-fold decreases. Among the significantly upregulated genes, *SMC3*, *CHD1*, *LINC01312*, *PLCB1*, *CHD1*, *ONECUT2*, *ARID4B*, *RNF34*, *USP47*, *RBBP8*, *STOX2*, *FBXL18*, *ZBTB20*, *CISD2*, *TP53BP1*, *USPL1*, *ZBTB10*, *CNTNAP5*, *SMC5*, *MIER3*, *TPR*, *TMTC4*, *GSK3B*, *SORL1*, *WHAMMP2*, and *WHAMMP3* displayed the greatest changes in expression, with >50-fold increases. In particular, the expressions of *SMC3* and *CHD1* were upregulated by >100 fold.

Enrichment analysis indicated that the transfection of PASMCs with HIF1α overexpression vectors contributed to the development and progression of thyroid cancer, endometrial carcinoma, glioma, colorectal cancer, non-small cell lung cancer, and chronic myelogenous leukemia. It also led to significant changes in stem cell pluripotency, ribosome- and ubiquitin-mediated protein degradation, adhesion plaques, calcium reabsorption, and the endocytosis signaling pathway. Transfection of HIF1α overexpression vectors into PASMCs also resulted in the following functional changes: RNA polymerase II transcription, mRNA binding, regulation of intracellular amino acid
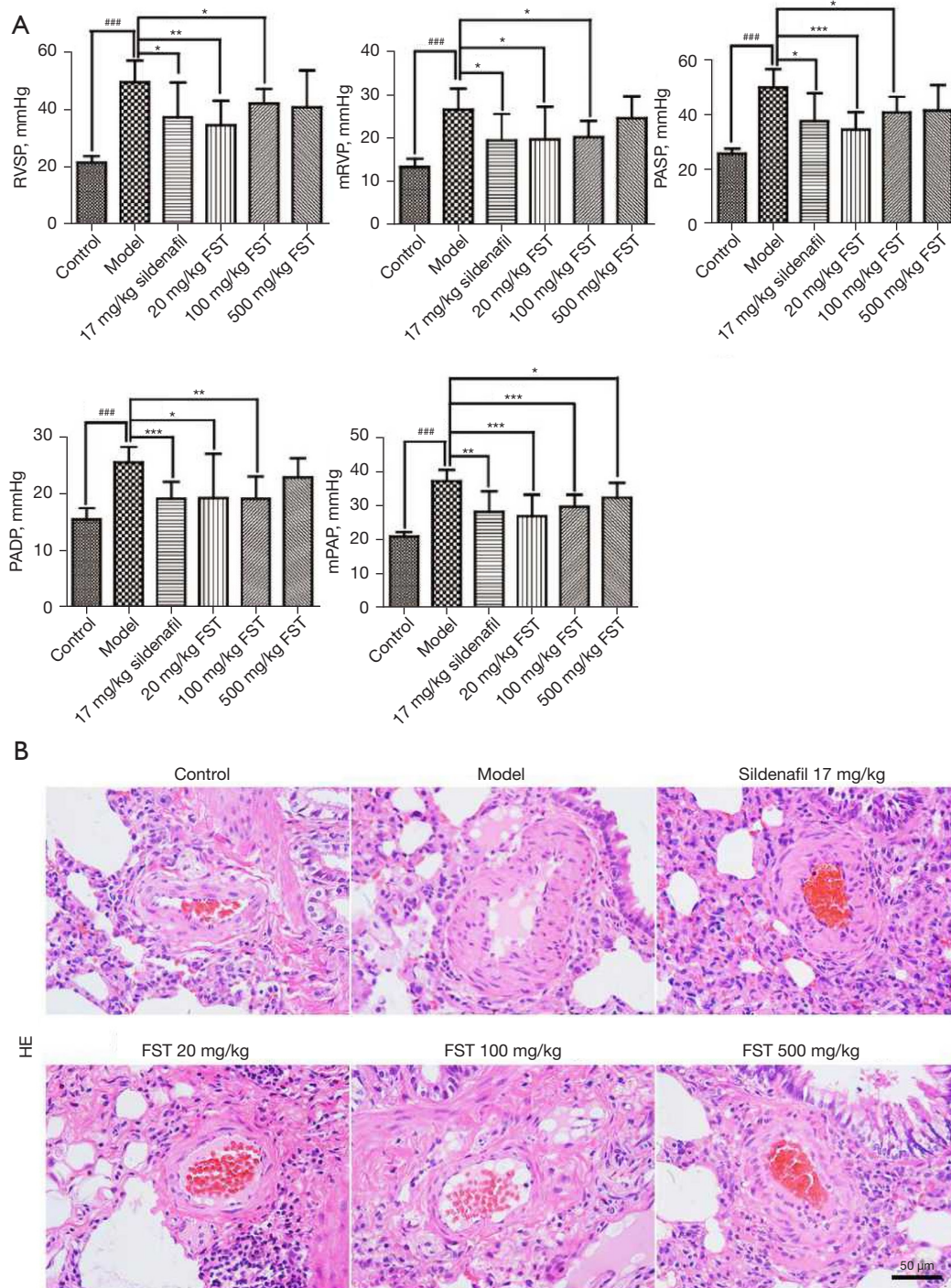
Figure 1 The protective effects of FST in rats with PH. (A) The effect of FST on physiological indexes in rats with PH. (B) The effect of FST on the pathological structure of lung tissue in rats with PH. Compared with the control group, ###, P<0.001; compared with the model group, ***, P<0.001, **, P<0.01, *, P<0.05. RVSP, right ventricular systolic pressure; FST, total flavones from *Sceptridium ternatum*; mRVP, mean right ventricular pressure; PASP, pulmonary artery systolic pressure; PADP, pulmonary artery diastolic pressure; mPAP, mean pulmonary arterial pressure; HE, hematoxylin and eosin; PH, pulmonary hypertension.
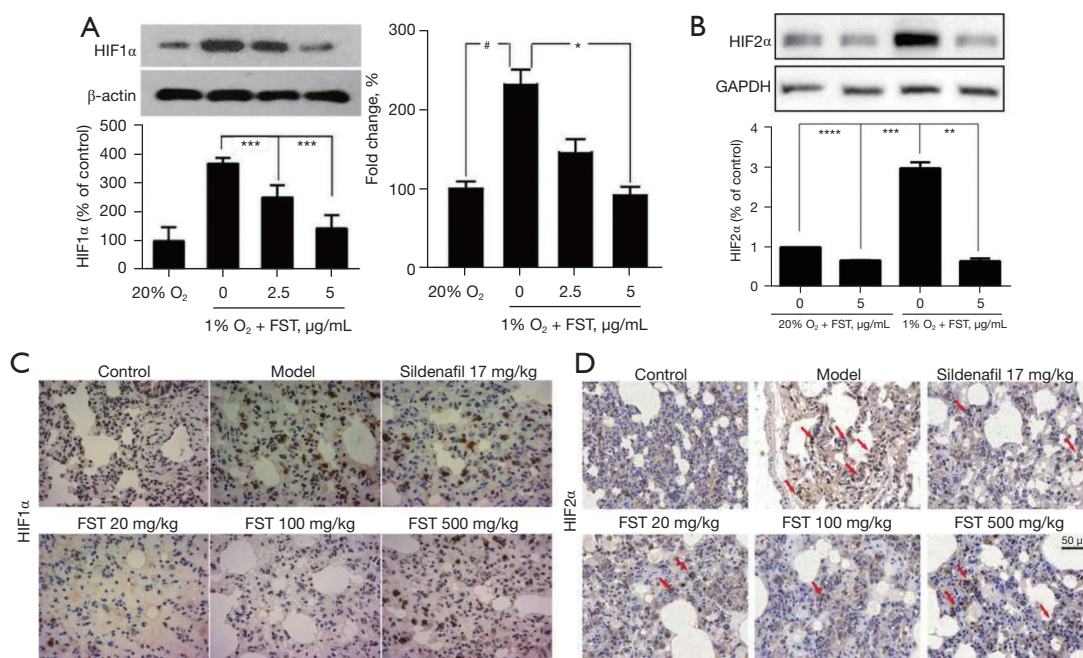
Figure 2 FST decreases the expression of HIF in PASMCs and the lung tissue of rats with PH. (A) The expression of HIF1α mRNA and protein in PASMCs. (B) The expression of HIF2α protein in HPMECs. (C) The expression of HIF1α in lung tissue of rats with PH, as detected by immunohistochemistry. Magnification: 400×. (D) The expression of HIF2α in lung tissue of rats with PH, as detected by immunohistochemistry. Magnification: 400×; the red arrows indicate a positive immunohistochemical stain. Compared with the hypoxic group with 1% O_2, *, P<0.05, **, P<0.01, ***, P<0.001, ****, P<0.0001; compared with the normal group with 20% O_2, #, P<0.05. FST, total flavones from *Sceptridium ternatum*; PASMCs, pulmonary artery smooth muscle cells; PH, pulmonary hypertension; HPMECs, human pulmonary microvascular endothelial cells.
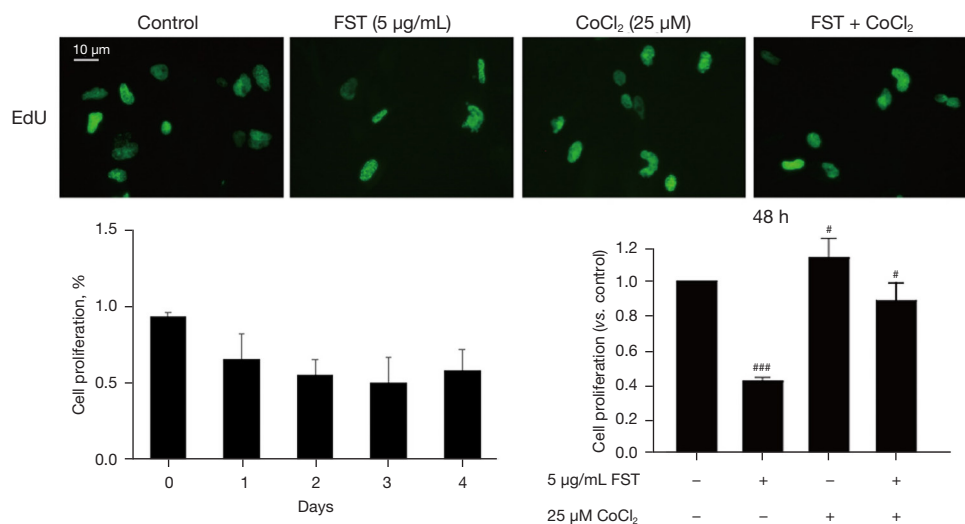

Figure 3 The effect of FST on the proliferation of vascular endothelial cells. Compared with the hypoxic group with 1% O_2, #, P<0.05, ###, P<0.001. The symbol (+) means it's added; the symbol (–) indicates that the substance is not added. EdU, 5-ethynyl-2'-deoxyuridine; FST, total flavones from *Sceptridium ternatum*.

Table 2 Top 49 downregulated genes in PASMCs after FST intervention

Gene symbol	Fold change
LOC554206	67.0
LOC101930657	61.4
PKP2	58.1
RBBP8	51.3
LSM5	50.5
FSIP2	50.4
CYP4A11/CYP4A22	49.3
SPON1	48.7
MTHFD2L	48.2
ZNF256	47.0
KCNB1	45.8
VRK1	45.6
WDR27	44.7
OR12D3/OR5V1	44.5
HAUS7/TREX2	43.9
CYBRD1	43.2
PTCH1	43.2
PARP2	42.3
GSK3B	41.1
DBT	40.8
CCDC152	40.1
MAP3K2	40.0
COG5	39.6
TP63	38.0
CA8	37.7
SPEF2	37.7
EML6	37.6
PIPOX	37.4
LOC101928707	36.0
USP37	35.8
LINC00865	35.6
TTF2	35.5
MAST2	35.3
MPZL3	34.8

Table 2 (*continued*)

Table 2 (*continued*)

Gene symbol	Fold change
SAP30BP	34.8
IRF2	33.4
PSEN1	33.4
LOC101929949	33.3
KCNJ15	33.3
UQCRH/UQCRHL	33.3
LOC400692	33.1
SMPD1	32.9
TPMT	32.1
EPHB4	30.7
CD58	30.3
SNX3	30.2
DNAJC6	30.2
CADM2	29.9
PNPLA3	29.4

PASMCs, pulmonary artery smooth muscle cells; FST, total flavones from *Sceptridium ternatum*.

metabolism, transcriptional inhibitor, ribonucleoprotein complex, ubiquitin ligase complex, multi-organ metabolism, regulation of viral gene expression, viral transcription, RNA connection, spliceosomal complex, post-transcriptional modification, DNA metabolism, and transferase complex.

Genes related to the mechanism of action of FST

Analysis of the differentially expressed genes indicated that after FST treatment, there were significant (≥3-fold) changes in the expression of 1,215 genes in PASMCs transfected with HIF1α plasmids. There were 611 downregulated genes and 604 upregulated genes (*Table 2* and *Table 3*, respectively). Of the significantly downregulated genes, *LOC554206*, *LOC101930657*, *PKP2*, *RBBP8*, *LSM5*, and *FSIP2* showed the greatest expression changes, with >50-fold decreases. Of the significantly upregulated genes, *VPS36*, *CDC5L*, *ST7-OT4*, *RPL5* (*SNORD21*), and *ZFP82* displayed the greatest expression changes, with >50-fold increases.

Further enrichment analysis (*Figure 4*) showed that after the transfection of PASMCs with the HIF1α plasmid, there

Table 3 Top 50 upregulated genes in PASMCs after FST intervention

Gene symbol	Fold change
VPS36	84.3
CDC5L	73.2
ST7-OT4	56.5
RPL5/SNORD21	54.6
ZFP82	54.6
SIX2	45.3
ALMS1	44.9
MRPL39	41.7
CCNT1	41.4
RIT1	41.2
ZNF253	40.8
NUDT16	40.0
MDM1	39.4
TOX4	38.9
SULF1	37.6
CSTF3	37.1
MAOB	36.7
ZFYVE28	36.4
ACOX1	35.8
ADAM18	34.9
PCYT1B	33.4
AKR1C3	33.3
KDM3B	33.1
LOC284561	32.9
IFRD1	32.5
DNAJC22	32.5
LOC728819	32.3
LRRC2-AS1	32.1
RAB18	32.0
LOC100506834	31.5
ATP6V1G2	31.2
AHI1	31.2
HSBP1	30.8
PCNT	30.7

Table 3 (*continued*)

Table 3 (*continued*)

Gene symbol	Fold change
PRKXP1	30.5
CREB1	30.5
MTHFD2L	30.4
KIAA1191	30.2
LOC100996634	30.1
CA5BP1	30.1
ZNF346	29.7
CTSC	29.1
ANXA11	29.0
RHEB	28.8
CAPN1	28.6
PIH1D2	28.3
MCUR1	28.0
TMEM50B	27.2
CCDC26	27.2
FBXW2	27.0

PASMCs, pulmonary artery smooth muscle cells; FST, total flavones from Sceptridium ternatum.

were significant changes observed in polysomes, protein complex scaffold, single-stranded DNA ligation reaction, core promoter sequence-specific DNA binding, core promotor binding, and messenger and RNA splicing. Kyoto Encyclopedia of Genes and Genomes (KEGG) enrichment analysis revealed changes in collecting duct acid section, *Vibrio cholerae* infection, and prostate cancer.

The HIF1α-related and FST-related gene subsets were selected, and the genes that are common but differentially expressed were obtained, and the genes with the opposite trend were taken as genes potentially related to the mechanism of FST based on HIF1α intervention. The results showed that 293 genes were significantly changed (≥3 times the variation) after HIF1α transfection and FST intervention, of which 161 genes showed the opposite trend and were candidate genes for subsequent research.

Enrichment analysis showed that transfection of PASMCs with HIF1α overexpression vectors induced embryonic development, RNA processing, mechanical stimulation, estradiol effect, senescence, cell differentiation, spermatogenesis, outflow tract formation, three tricuspid
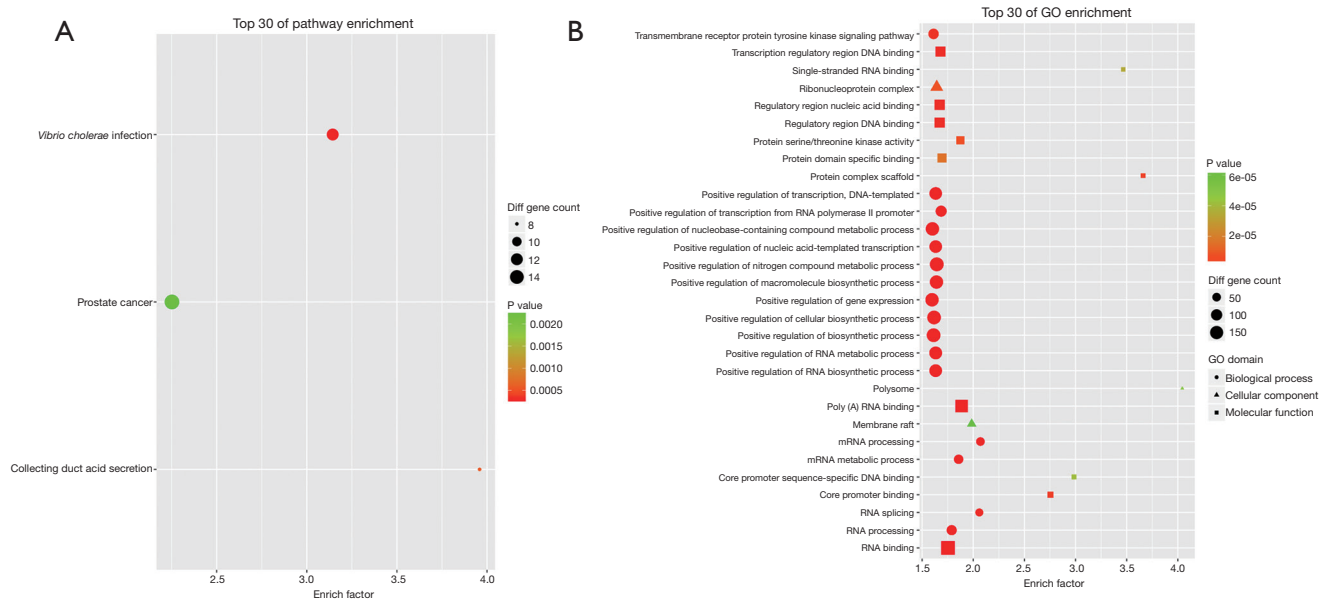
Figure 4 Intervention mechanism of FST. (A) GO enrichment analysis of differentially expressed genes after FST intervention in PASMCs transfected with HIF1α plasmids. (B) KEGG enrichment analysis of differential gene after FST intervention in PASMCs transfected with HIF1α plasmids. GO, Gene Ontology; FST, total flavones from *Sceptridium ternatum*; PASMCs, pulmonary artery smooth muscle cells; KEGG, Kyoto Encyclopedia of Genes and Genomes.

septal formation, atrioventricular valve formation, activation of epidermal growth factor receptor (EGFR) negative regulation, linolenic acid metabolism, the Smo signaling pathway, and RNA polymerase II promoter transcriptional negative regulation function change. KEGG enrichment revealed that genes regulated by HIF1α overexpression and negatively regulated by FST was closely related to changes in CYP450 drug metabolism, chemical carcinogenesis, endoplasmic reticulum protein processing, and viral carcinogenesis (*Figure 5* and *Tables 4,5*). Further, specific pathway analysis based on KEGG and Gene Ontology (GO) analyses revealed MAPK, JAK-STAT, and HDAC to be key pathways (*Figure 6A*). By considering the changes in gene expression, functional analysis results, and previous research findings, we preliminarily screened *SOCS1*, *STAT3*, *CACNG4*, *RASSF8*, *SMAD5*, *DUOXA1*, *CACNA1I*, *KALRN*, *TGFBR2*, and *ASB3* (*AX747197*) gene as downstream genes in the mechanism of FST for further validation (*Figure 6B*).

Verification of candidate genes by RT-qPCR

Key genes in different signaling pathways screened from the hypoxic cell model were verified by RT-qPCR. The

results showed that the mRNA expression levels of all tested genes were basically consistent with the microarray data (*Figure 6C*). Therefore, the microarray data were suitable for signaling pathway mining. Furthermore, the expression levels of JAK2-STAT3 signaling pathway genes and the downstream negative regulator *SOCS1* were also changed. This observation implied that the protective effects of FST on PASMCs might be related to this pathway, although more verification is needed.

Effects of FST on the JAK2-STAT3 signaling pathway

Effects in PASMCs

The JAK-STAT signaling pathway is an important pathway involved in cell proliferation, differentiation, apoptosis, and aging. To study the effects of FST on the JAK-STAT signaling pathway, we detected the expression of JAK-STAT signaling pathway genes, and the results are shown in *Figure 7*. Compared with normoxic cells, hypoxic cells had significantly increased phosphorylation levels of JAK2 and STAT3, while the expression level of *SOCS1*, the transcription factor downstream of JAK2 and STAT3, was decreased significantly. These observations indicated that hypoxia activated the JAK2-STAT3 signaling pathway. In

Figure 5 Genes related to the mechanism of action of FST. (A) FST downregulates the genes upregulated by HIF1α. (B) FST upregulates the genes downregulated by HIF1α. FST, total flavones from *Sceptridium ternatum*.

contrast, FST treatment effectively inhibited the expression of p-JAK2 and p-STAT3 in hypoxic cells (P<0.05) but increased that of their negative regulator SOCS1 (P<0.001); in short, the activation of the JAK2-STAT3 signaling pathway was significantly inhibited.

Effects in lung tissues of rats with PH

To observe the effects of FST on the JAK2-STAT3 signaling pathway *in vivo*, an MCT-induced PH model was established in SD rats. Immunohistochemical staining was performed on lung tissues from the rats and changes in

Table 4 Genes upregulated by transfection with HIF1α overexpression vectors and downregulated by FST intervention

Gene symbol	Fold changes	
	Downregulated by FST	Upregulated by HIF1α
ZNF365	47	16.5
PAWR	42.3	6.8
HCG18	41.1	24.4
KALRN	33.4	6.9
MARVELD1	23	6.3
WBP11	22.8	4.6
SSR1	20.3	3.2
PTCH1	20.2	11
PENK	19.3	10.8
CASC7	17.6	4.8
TGFBR2	17.4	11.5
THAP4	16.8	3.6
ASB3	15.4	9.7
SREK1	4.8	3
FGD6	4.4	4.9
GDF11	3.4	8.8
ADH5	3.4	4.5
CNTNAP5	3.2	54.3
POM121L2	4.9	12.3
ABCA2	14.2	9.8
ANKRD10	13.7	6.9
KLF5	13.1	4.4
ZNF644	10.7	17.3
ABCA9	9.8	6.9
SMOC2	9.2	4.9
CNNM3	8	4.5
PIEZO2	7.1	3.3
SUZ12	6.9	9
STAT3	6.7	13.3
SERTM1	6.4	5.1
ZBTB10	5.9	55.3
VEZF1	5.2	7.4
ZNFX1	4.3	9.7

Table 4 (*continued*)

Table 4 (*continued*)

Gene symbol	Fold changes	
	Downregulated by FST	Upregulated by HIF1α
SOCS5	3.4	7.8
DHX9	3.2	9.4
PARP2	3.1	26.5
DDAH2	3	12.6

FST, total flavones from *Sceptridium ternatum*.

Table 5 Genes downregulated by transfection with HIF1α overexpression vectors and upregulated by FST intervention

Gene symbol	Fold changes	
	Upregulated by FST	Downregulated by HIF1α
ACOX1	35.8	9.2
ACTN2	24.6	30.8
ADAM18	34.9	12.8
ADAMTS5	12.6	3.9
AHI1	22.2	45.7
AK021804	31.2	14.6
ALDH3B1	33.3	3.9
ANXA9	29.0	17.2
ARHGEF7-AS2	9.9	4.2
ATP6V1D	10.0	9.3
ATP9B	8.5	4.2
BCKDHB	6.2	4.2
BMPR1A	8.5	6.8
C15orf41	18.6	15.5
C1orf54	9.1	7.7
CA5BP1	3.9	7.4
CACNA1I	30.1	4.0
CACNG4	3.1	5.8
CAPN1	15.6	5.4
CAPN2	28.6	4.0
CASC10	3.0	6.2
CBX3P2	11.3	4.9
CCDC47	27.2	3.9
CD244	10.0	3.0

Table 5 (*continued*)

Table 5 (*continued*)

Gene symbol	Fold changes	
	Upregulated by FST	Downregulated by HIF1α
CENPN	7.7	4.6
CR1	3.3	7.3
CREB3L2	3.7	10.0
CSMD1	5.3	21.2
CTSC	17.6	3.2
DAZ1/2/3/4	29.1	33.1
DBF4	25.2	10.4
DCAF6	17.0	10.8
DENR	5.6	9.0
DICER1	13.0	15.5
DUOXA1	14.8	6.1
DYRK2	9.7	3.1
EIF3D	10.5	3.7
EIF5	5.6	12.9
RAB18	19.2	47.8
RAD23B	15.2	11.5
RASSF8	3.8	5.9
RECK	11.0	28.6
RHOF	4.6	9.6
RIMKLA	15.8	8.0
RNF144A-AS1	5.6	12.2
RRNAD1	4.6	7.7
SDK1	13.7	3.1
TAB2	5.6	4.1
TACR3	8.5	11.9
TAF15	3.7	20.7
TMEM50B	10.6	5.5
TMTC1	27.2	35.5
XRCC6BP1	8.2	3.1
ZBTB22	6.6	3.3
ZBTB24	20.3	25.0
ZFPM2	25.1	11.9
ZFYVE28	8.8	18.0
ELOVL5	8.4	7.1

Table 5 (*continued*)

Table 5 (*continued*)

Gene symbol	Fold changes	
	Upregulated by FST	Downregulated by HIF1α
FLJ33544	4.3	17.0
GPR1	25.4	19.1
HDAC8	4.9	3.7
HDGF	5.3	3.1
HDGFRP3	3.2	3.8
HEYL	11.0	3.6
HIST2H2BE	3.3	13.0
HNRNPDL	3.3	3.0
HSPA12B	8.6	3.2
IDH1-AS1	6.0	3.0
IFNGR1	13.5	38.9
IGSF6	4.0	5.2
KLHL22	5.4	43.8
LIN7A	11.6	30.0
LRRC2-AS1	5.3	29.7
MGEA5	8.3	10.7
MGST3	5.5	4.4
MIB2	4.7	5.4
MICAL3	3.7	5.8
MIPEPP3	3.2	14.3
MRPL34	5.4	3.1
MRPS15	5.6	3.2
MS4A3	4.3	23.9
MSS51	5.1	4.3
NHLH1	9.3	3.1
NNT	6.8	22.6
NR5A2	13.3	8.9
NRF1	6.3	6.9
NUDT16	10.0	6.6
NUPL1	40.0	19.2
OLFML3	12.6	19.8
OR11A1	3.2	22.5
PDGFRL	3.9	5.5
PPP1R12B	4.2	17.2

Table 5 (*continued*)

Table 5 (*continued*)

Gene symbol	Fold changes	
	Upregulated by FST	Downregulated by HIF1α
PRKCH	11.3	34.3
PRKXP1	13.7	31.1
QRSL1	10.5	17.8
SEC23A	11.5	14.0
SFT2D1	9.4	24.6
SGK494	19.7	22.4
SLC16A1-AS1	7.9	7.0
SLC17A6	3.9	7.3
SLC28A1	19.0	38.1
SLC5A12	7.2	3.4
SLITRK5	10.0	7.7
SMAD5	5.5	26.9
SOC1	4.6	10.6
SP140L	7.7	10.4
SYNJ2	3.6	5.2
TMX3	14.8	9.9
TNRC18	5.2	3.9
TOX4	11.1	21.9
TUBA4B	22.6	9.9
UGT1A6	3.1	13.8
USP25	20.4	3.3
XRCC5	4.1	3.3

FST, total flavones from *Sceptridium ternatum*.

the JAK2-STAT3 signaling pathway and its downstream negative regulator SOCS1 were observed. HE stains immunoreactive cells brown and nuclei deep purple.

Immunohistochemistry revealed no significant changes in the expression of JAK2 in the small pulmonary vascular wall between rats with PH in different groups. In the normal control group, p-JAK2 was not positively expressed, although it was considerably upregulated in the PH model group. After FST treatment (20, 100, and 500 mg/kg), p-JAK2 expression was decreased to varying extents as compared with the model group. Experimental results showed that MCT induced the phosphorylation of the connexin JAK2, while FST reduced the expression

of p-JAK2. Compared with those in the negative control group, rats in the PH model and FST treatment groups exhibited more STAT3 in the nuclei of the small pulmonary vascular wall. Immunohistochemistry of p-STAT3 showed that p-STAT3 was basically not expressed in the lung tissues of the normal control group. In contrast, p-STAT3 was positively expressed in the small pulmonary vascular wall of the PH model rats. Positive particles were mainly localized in the nuclei (which was consistent with HE staining), with a few in the cytoplasm. Compared with that in the model group, p-STAT3 expression in the different FST treatment groups was decreased considerably. Our experimental results indicated that MCT induced the phosphorylation of STAT3, while FST treatment inhibited the MCT-induced expression of p-STAT3. Immunohistochemical results showed that SOCS1 expression was decreased considerably in the lung tissues of the model group compared with the normal control group. In contrast, after FST treatment at different doses, SOCS1 expression was significantly increased. These results suggested that FST increased the expression of the negative regulator SOCS1 downstream of the JAK2-STAT3 signaling pathway (*Figure 8A*).

As shown in *Figure 8B*, the expression levels of p-JAK2 and p-STAT3 were increased considerably (P<0.01), while the expression of SOCS1 was decreased (P<0.05) in the lung tissues of the PH model group. Compared with the model group, the FST treatment groups exhibited significant decreases in the expression of p-JAK2 and p-STAT3 (P<0.01), but significant increases in SOCS1 expression (P<0.05), in a dose-dependent manner. These findings were in line with the *in vitro* experimental results, further confirming the role of the JAK-STAT signaling pathway in the action mechanism of FST against PH.

Discussion

In our preliminary research, we demonstrated that FST could reverse the hypoxia-induced proliferation of PASMCs. *In vitro* study had also indicated that FST could considerably alleviate MCT-induced PH in rats. However, the working mechanism of FST against PH remained unclear, so the present study set out to conduct an in-depth mechanistic analysis.

We found that FST significantly inhibited the expression of HIF1α in a hypoxia-induced cell model and lung tissues of rats with PH. Under normoxic conditions, HIF1α is extremely likely to degrade (6,9), with a half-life shorter than 5 minutes. However, under hypoxic conditions, it
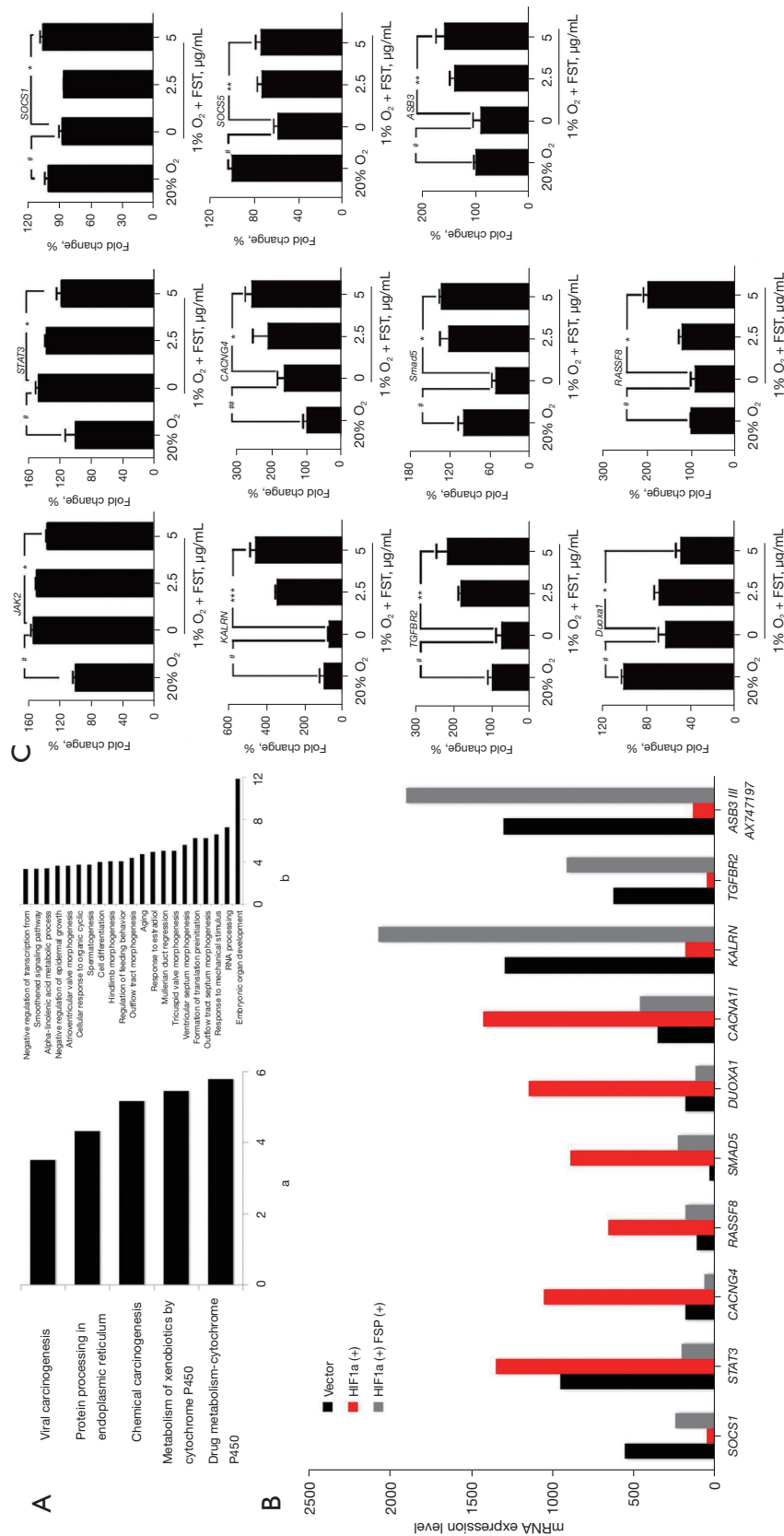
Figure 6 Verification of candidate genes related to the mechanism of action of FST. (A) Function and pathway enrichment maps of genes regulated by HIF1α overexpression and negatively regulated by FST: (a) KEGG pathway enrichment map; (b) GO pathway enrichment map. (B) Candidate genes related to PH were screened by gene microarray. (C) The mRNA expression of candidate genes in PASMCs was verified by RT-qPCR. Compared with the hypoxia group with 1% O_2, *, $P<0.05$, **, $P<0.01$, ***, $P<0.001$; compared with the normal group with 20% O_2, #, $P<0.05$, ##, $P<0.01$. FST, total flavones from *Sceptridium ternatum*; KEGG, Kyoto Encyclopedia of Genes and Genomes; GO, Gene Ontology; PH, pulmonary hypertension; PASMCs, pulmonary artery smooth muscle cells; RT-qPCR, real-time quantitative PCR.
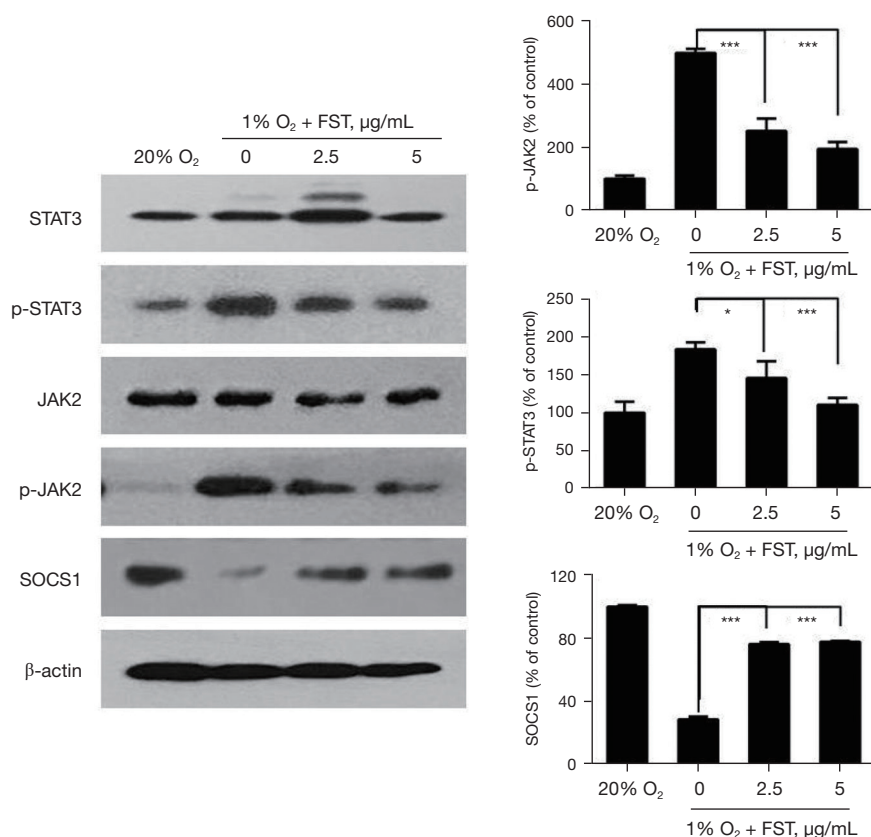
Figure 7 Effects of FST on JAK2-STAT3 signaling pathway-related proteins in PASMCs detected by western blot. Compared with the hypoxia group with 1% O$_2$, *, P<0.05, ***, P<0.001. FST, total flavones from *Sceptridium ternatum*; PASMCs, pulmonary artery smooth muscle cells.

exhibits a dramatic increase in stability and transcriptional activity, and participates in the regulation of cell apoptosis and autophagy, endoplasmic reticulum stress, and inflammation. Our results indicated that overexpression of HIF1α under hypoxia was involved in the working mechanism of FST against PH.

In the present study, HPASMCs were transfected with HIF1α overexpression vectors, and the hypoxic environment in PH was mimicked on the genetic level. A subset of differentially expressed genes induced by the upregulation of HIF1α was compared with a subset of genes significantly affected by FST treatment. The results showed that expression of signaling pathways related to cell proliferation, differentiation, and apoptosis, and those mediating immune dysregulation and tumorigenesis has been found to change significantly (10,11). The expression of the JAK2-STAT3 signaling pathway and its downstream negative regulator SOCS1 differed significantly in the FST

treatment groups (12). JAK2 is a member of the protein tyrosine kinase family, and p-JAK2 can enter the nuclei and mediate the signaling cascade related to the binding of cytokines to the receptors. The transcription activator STAT3 is a downstream target gene of JAK2 and plays an important role in the maintenance of cell self-renewal (13,14). Under pathological conditions, PH can lead to excess proliferation of PASMCs, while inhibiting excess cell self-renewal; this mechanism can be utilized in the treatment of PH (15,16). We speculated that the JAK2-STAT3 signaling pathway is an important pathway in the HIF1α-mediated effect of FST against PH.

To confirm the above hypothesis, experiments were performed to detect the expression of JAK2-STAT3 and its negative regulator SCOS1 in hypoxia-treated cells. After FST treatment, the mRNA and protein expression levels of JAK2 and STAT3 were observed to be downregulated in hypoxic cells. This increased the expression of SOCS1,
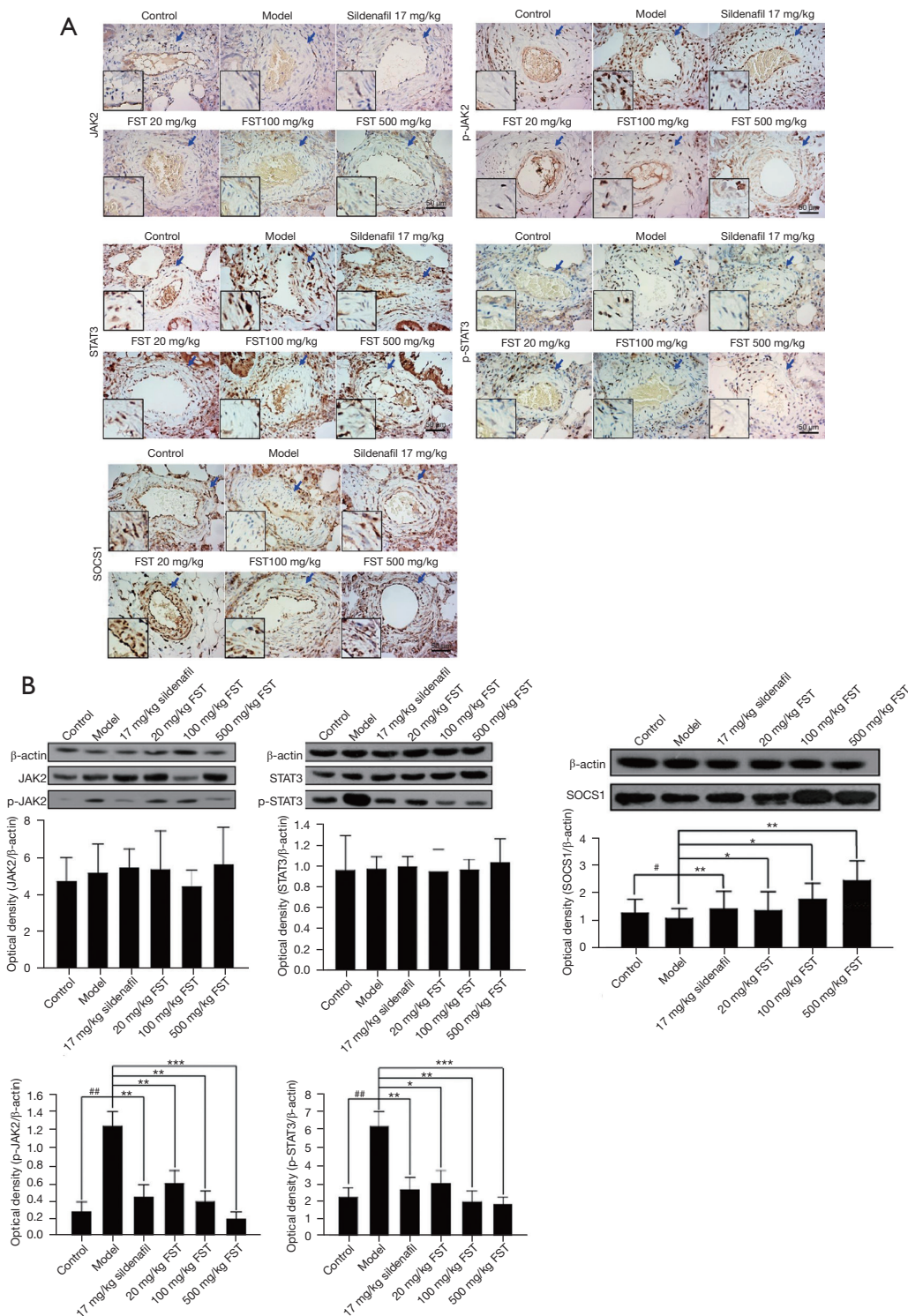
Figure 8 Effects of FST on the JAK2-STAT3 signaling pathway in lung tissue of rats with PH. (A) The effect of FST on the expression of JAK2-STAT3 and SOCS1 in lung tissue of rats with PH, as detected by immunohistochemistry. 400× before amplification; 1,000× in small box. The blue arrow indicates the magnified area. (B) The effect of FST on the expression of JAK2-STAT3 and SOCS1 in lung tissue of rats with PH, as detected by western blot. Sildenafil as a positive control group. Compared with the model group, *, $P<0.05$, **, $P<0.01$, ***, $P<0.001$; compared with the control group, #, $P<0.05$, ##, $P<0.01$. FST, total flavones from *Sceptridium ternatum*; PH, pulmonary hypertension.

which in turn further downregulated JAK2-STAT3. The phosphorylated forms of JAK2-STAT3 and SCOS1 were also inhibited. The above results were verified in a rat model of PH. Immunohistochemistry indicated no significant changes in the expression of JAK2 between the groups; however, the expression of p-JAK2 showed considerable differences and was decreased by FST treatment regardless of the dose. Further, FST inhibited the entry of STAT3 into the nuclei and reduced the expression of p-STAT3 while upregulating SOCS1 expression, which was consistent with the *in vitro* results. Similar results were also obtained from western blot. Thus, the regulatory effect of FST on the JAK2-STAT3 signaling pathway and SOCS1 was confirmed in both the animal and cell models. From these results, it could be inferred that FST exerted its effects against PH through the JAK2-STAT3 signaling pathway. However, although expression data were obtained for several potential downstream mediators of FST, these data were not adequate to claim causality. Therefore, we used $CoCl_2$ intervention to establish a hypoxic model and used IL-6 for the promotion of PASMC proliferation and reverse validation. The expression of STAT3 and p-STAT3 was detected by western blot, and the results showed that FST could significantly reduce the expression of p-STAT3, which is the main active form of STAT3, thus further clarifying the therapeutic mechanism of FST in PH. This study showed that the high expression of HIF1α and HIF2α, and the activation of JAK2-STAT3 signaling pathway can be used for early diagnosis, disease evaluation and prognosis of PH.

Conclusions

This study has uncovered the working mechanism of FST against PH using microarray analysis and has verified the effect of FST on key signaling pathways, both *in vitro* and *in vivo*. Our experimental results show that FST intervention downregulates the expression of HIF1α and HIF2α, which are related to the occurrence and development of PH, and inhibits the activation of the downstream JAK2-STAT3 signaling pathway, which in turn suppresses the proliferation of HPASMCs and HPASMCs to alleviate the pathological symptoms of PH. The working mechanism and molecular targets of FST in PH have thus been identified from the pharmacological perspective.

Acknowledgments

Footnote

Reporting Checklist: The authors have completed the ARRIVE reporting checklist. Available at https://atm.amegroups.com/article/view/10.21037/atm-21-5889/rc

Data Sharing Statement: Available at https://atm.amegroups.com/article/view/10.21037/atm-21-5889/dss

Conflicts of Interest: All authors have completed the ICMJE uniform disclosure form (available at https://atm.amegroups.com/article/view/10.21037/atm-21-5889/coif). The authors have no conflicts of interest to declare.

Ethical Statement: The authors are accountable for all aspects of the work in ensuring that questions related to the accuracy or integrity of any part of the work are appropriately investigated and resolved. Experiments involving animals were performed under a project license (No. 0273015) granted by the ethics institutional review board of Zhejiang Cancer Hospital, in compliance with Regulations for the Administration of Affairs Concerning Experimental Animals (modified in 2017) for the care and use of animals.

Open Access Statement: This is an Open Access article distributed in accordance with the Creative Commons Attribution-NonCommercial-NoDerivs 4.0 International License (CC BY-NC-ND 4.0), which permits the non-commercial replication and distribution of the article with the strict proviso that no changes or edits are made and the

References

1. Ataya A, Barretto J, Wynne J. Pulmonary Hypertension. Am J Respir Crit Care Med 2015;192:1514-6.
2. Thenappan T, Ormiston ML, Ryan JJ, et al. Pulmonary arterial hypertension: pathogenesis and clinical management. BMJ 2018;360:j5492.
3. Lévy M, Maurey C, Celermajer DS, et al. Impaired apoptosis of pulmonary endothelial cells is associated with intimal proliferation and irreversibility of pulmonary hypertension in congenital heart disease. J Am Coll Cardiol 2007;49:803-10.
4. Wang Y, Yan L, Zhang Z, et al. Epigenetic Regulation and Its Therapeutic Potential in Pulmonary Hypertension. Front Pharmacol 2018;9:241.
5. Lu A, Zuo C, He Y, et al. EP3 receptor deficiency attenuates pulmonary hypertension through suppression of Rho/TGF-β1 signaling. J Clin Invest 2015;125:1228-42.
6. Makino Y, Cao R, Svensson K, et al. Inhibitory PAS domain protein is a negative regulator of hypoxia-inducible gene expression. Nature 2001;414:550-4.
7. Ying Y, Ye ZW, Huang P, et al. Sceptridium Ternatum For the Treatment of Pulmonary Arterial Hypertension in Rats with Pulmonary Heart. Chinese Journal of Modern Applied Pharmacy 2014;31:790-4.
8. Wang M, Chen DQ, Chen L, et al. Novel RAS Inhibitors Poricoic Acid ZG and Poricoic Acid ZH Attenuate Renal Fibrosis via a Wnt/β-Catenin Pathway and Targeted Phosphorylation of smad3 Signaling. J Agric Food Chem 2018;66:1828-42.
9. Pawlus MR, Hu CJ. Enhanceosomes as integrators of hypoxia inducible factor (HIF) and other transcription factors in the hypoxic transcriptional response. Cell Signal 2013;25:1895-903.
10. Langen RC, Gosker HR, Remels AH, et al. Triggers and mechanisms of skeletal muscle wasting in chronic obstructive pulmonary disease. Int J Biochem Cell Biol 2013;45:2245-56.
11. Vorrink SU, Domann FE. Regulatory crosstalk and interference between the xenobiotic and hypoxia sensing pathways at the AhR-ARNT-HIF1α signaling node. Chem Biol Interact 2014;218:82-8.
12. Cittadini A, Monti MG, Iaccarino G, et al. SOCS1 gene transfer accelerates the transition to heart failure through the inhibition of the gp130/JAK/STAT pathway. Cardiovasc Res 2012;96:381-90.
13. Xu Y, Lv SX. The effect of JAK2 knockout on inhibition of liver tumor growth by inducing apoptosis, autophagy and anti-proliferation via STATs and PI3K/AKT signaling pathways. Biomed Pharmacother 2016;84:1202-12.
14. You L, Wang Z, Li H, et al. The role of STAT3 in autophagy. Autophagy 2015;11:729-39.
15. Breitling S, Ravindran K, Goldenberg NM, et al. The pathophysiology of pulmonary hypertension in left heart disease. Am J Physiol Lung Cell Mol Physiol 2015;309:L924-41.
16. Rowan SC, Keane MP, Gaine S, et al. Hypoxic pulmonary hypertension in chronic lung diseases: novel vasoconstrictor pathways. Lancet Respir Med 2016;4:225-36.